Surface Protolysis and Its Kinetics Impact the Electrical Double Layer

Max F. Döpke,[1] Fenna Westerbaan van der Meij,[1] Benoit Coasne,[2] and Remco Hartkamp[1,*]
[1]Process & Energy Department, Delft University of Technology, Leeghwaterstraat 39, 2628 CB Delft, Netherlands
[2]Université Grenoble Alpes, CNRS, LIPhy, 38000 Grenoble, France

(Received 14 September 2021; revised 8 December 2021; accepted 5 January 2022; published 2 February 2022)

Surface conductivity in the electrical double layer (EDL) is known to be affected by proton hopping and diffusion at solid-liquid interfaces. Yet, the role of surface protolysis and its kinetics on the thermodynamic and transport properties of the EDL are usually ignored as physical models consider static surfaces. Here, using a novel molecular dynamics method mimicking surface protolysis, we unveil the impact of such chemical events on the system's response. Protolysis is found to strongly affect the EDL and electrokinetic aspects with major changes in ζ potential and electro-osmotic flow.

DOI: 10.1103/PhysRevLett.128.056001

Solid-liquid interfaces, which are omnipresent in nature, are central to many scientific fields such as colloid or materials science, phase separation or catalysis, and electrochemistry or energy harvesting. A detailed understanding of such interfaces is of paramount importance to design novel energy devices (e.g., batteries, osmotic power membranes) and innovative health or environment applications (e.g., drug delivery capsules, medium depollution or remediation). Solid-liquid interfaces are characterized by two parallel layers of equal charge and opposite polarity known as the electrical double layer (EDL) [1]. The electric charge distribution across these layers is usually described via mean-field models, which disregard the microscopic intricacies of the interfacial structure and chemistry. Beyond such pioneering approaches, researchers have proposed ways to effectively account for molecular details including ion-specific effects, microscopic correlations, and surface charge localization. In contrast, despite its acknowledged interplay with the EDL, surface reactivity is not included in available frameworks. In particular, proton exchange at oxide-electrolyte interfaces, which directly influences hydrogen hopping and diffusion and, hence, surface conductivity [2,3], is usually disregarded in modeling endeavors as it is implicitly assumed that surface charge distributions evolve too slowly to affect the interfacial fluid structure and dynamics.

Experimentally, proton exchange rates can only be measured from the interface transient response to an applied perturbation such as with pressure-jump techniques [4]. However, with most methods, only lower bounds or orders of magnitude can be estimated for such reaction rates. For instance, in atomic force microscopy experiments on silica with tip speeds as fast as 0.5 μm/s, charge regulation due to the EDL overlap between the surface and tip is so fast that no hysteresis is observed in force-distance curves [5]. This suggests that surface chemistry adapts within milliseconds—a value consistent with flow experiments on mineral surfaces probing the electronic response induced by composition changes [6–8]. Dissolution experiments also provide lower bounds for protolysis rates. To form a $Si(OH)_4$ molecule from a SiO_4 tetrahedron in SiO_2, multiple hydrolysis ($MOM + H_2O \rightleftharpoons MOH + MOH$) and protolysis ($MOH \rightleftharpoons MO^- + H^+$) reactions occur [9] (with protolysis being very fast and nearly activationless compared to hydrolysis [10]). Dissolution rates of 10^{-7} mol/m^2/s for silica under neutral pH, thus serve as a lower bound for surface protolysis rates [11,12]. Despite such estimates, exact equilibrium protolysis rates and their influence on the EDL cannot be experimentally probed.

Theoretically, while first-principles calculations provide insights into reaction mechanisms, energy barriers, and adsorption energies, the small system sizes in these approaches [O(10–100 atoms)] are insufficient to study the fluid response [13–17]. On the other hand, classical molecular dynamics (MD) simulations [$O(10^3 - 10^5)$ atoms] probe the fluid response, but they generally do not account for chemical reactions. Only recently, the computational power has increased to allow atomistic MD simulations to probe chemical reactions and fluid responses. In this context, the reactive force field ReaxFF [18] is an important landmark but parameters for protolysis are not available. In contrast, the dissociative force field MGFF [19,20] allows reproducing OH bond dissociation or formation involved in proton reactions. Using this force field, when set in contact with water, protolysis rates up to 2×10^5 mol/m^2/s were found for hydroxylated silica surfaces containing strained sites [Si(OH)Si and $SiOH_2$ defects], while smaller rates between 900 and 1750 mol/m^2/s were assessed when only considering silanol sites (SiOH) [21,22]. The OH bond lifetime was found to be broadly distributed from fs to ns with an average of the order of ps. Despite its

ability to model silanol dissociation, the MGFF force field is unsuitable to study the impact of reaction kinetics on the EDL as ion parameters are not available.

In this Letter, we first develop a novel framework to include surface reactions in classical MD simulations at no additional computational cost. This is achieved by adding every t_r time in the MD simulation a stochastic deprotonation and protonation step between two randomly picked, independent surface sites (one protonated, one deprotonated). Using this effective yet robust strategy, we then investigate the impact of proton exchange and its kinetics on the EDL formed in a prototypical silica-electrolyte system. We find that both the ion distribution and dynamics within the EDL are strongly impacted by proton exchange with significant effects on the system's electrokinetic response. By analyzing the molecular mechanisms of ion diffusion within the EDL, we unravel that ion adsorption times become much shorter when surface protolysis is taken into account while the water structure and dynamics are only indirectly impacted through the electrostatic coupling with ions.

Using the LAMMPS package [23], we implemented protonation or deprotonation reactions of the form $\mathrm{MOH} \rightleftharpoons \mathrm{MO^-} + \mathrm{H^+}$ in MD simulations by adjusting the partial charges and Lennard-Jones parameters of a $\mathrm{MO^-}$ group to a MOH group and vice versa. As shown in Fig. 1(a), without explicitly forming or breaking OH bonds, this strategy mimics equilibrium situations in which no net adsorption or desorption takes place—protonation and deprotonation always occur simultaneously. In doing so, direct proton exchange between MOH and $\mathrm{MO^-}$ sites avoids dealing with free protons and/or water ionization reactions while maintaining a constant overall surface charge. In principle, protonation and deprotonation could be treated as decoupled from each other using a canceling background charge. However, the use of concomitant protonation and deprotonation allows imposing a thermodynamic ensemble with well-defined constant parameters (surface charge, number of particles, temperature, and overall charge neutrality). As shown in Fig. 1(c), various reaction rates r can be considered by performing protolysis reactions at different time intervals $t_r \sim 1/r$ (see Table SI of the Supplemental Material [24], upon decreasing t_r, the simulation time step was decreased to ensure numerical stability). This implementation does not account for mutual coupling between fluid structure and surface chemistry. In reality, the probability to protonate or deprotonate a site depends on its environment at a given time. In principle, these probabilities can be calculated using, for example, reactive force fields such as those cited above. However, calculating an instantaneous energy landscape on the fly leads to prohibitive computational costs and statistical challenges. Moreover, including explicit water ionization reactions and water ions (10^{-6} mol/L for $\mathrm{H^+/H_3O^+}$ and 10^{-8} mol/L for $\mathrm{OH^-}$ in bulk at neutral pH) is out of reach (even for large MD systems like here, the number of water ions is too small to ensure statistical significance). To circumvent such issues, we use here an effective approach by stochastically selecting the surface groups to react at a given time. With such a coarse-grained description, we neglect (i) mechanisms occurring on a time shorter than the chemistry timescale (1–10 fs), (ii) possible electric screening of surface sites by lingering protons ($\mathrm{H^+}$) or hydroniums ($\mathrm{H_3O^+}$), and (iii) the fact that protonation and deprotonation occur independently. These simplifications may result in overpredicting the impact of surface reactions but we expect such coarse graining to be relevant as we only probe molecular events occurring in the EDL at longer times. Finally, to guarantee numerical stability, the parameter change between MOH and $\mathrm{MO^-}$ groups—which allows mimicking concomitant protonation and deprotonation—is linearly adjusted over 1 ps.

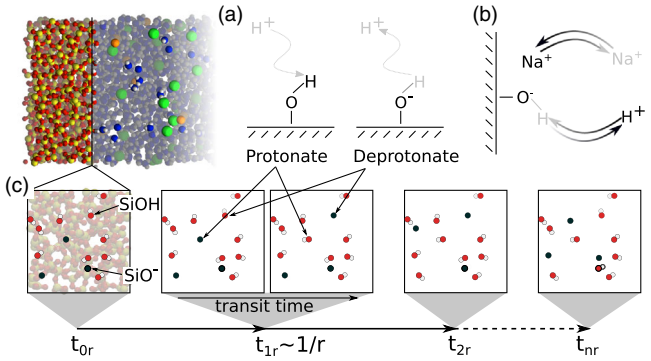

FIG. 1. (a) Schematic view of protonation and deprotonation reactions at solid-liquid interfaces. Black font indicates interatomic interactions are turned on, while gray font indicates these are turned off. (b) Protolysis reactions impact ion adsorption by allowing an ion to adsorb after site deprotonation (black) or forcing it to desorb after site protonation (gray). (c) Simulation protocol flow diagram with time $t_r \sim 1/r$ between protolysis reactions. Protonation and deprotonation events take place over a transit time to ensure numerical stability.

As a benchmark, we selected a prototypical amorphous silica slit pore of approximately 6 nm height filled with a 0.66–0.74 mol/L NaCl aqueous solution. Details on the setup and force fields can be found in the Supplemental Material [24], which includes Refs. [25–42]. The reaction rate r was varied between no reactions (nonreactive MD, equivalent to $r < 1.68$ mol/m^2/s for our simulation size and time) and $r = 10^4$ mol/m^2/s. For reference, protolysis rates on silica-water interfaces were estimated in Ref. [21] to be of the order of 10^2–10^5 mol/m^2/s using dissociative MD. Given the surface area [12.4 nm^2] and silanol density [4.7 SiOH/nm^2] in our system, protonation and deprotonation take place between every > 100 ns and 13.43 ps (see Table SI in Ref. [24]). In comparison, as shown below, $\mathrm{Na^+}$ residence times are of the order of a few hundred ps so that we expect a non-negligible rate dependence.

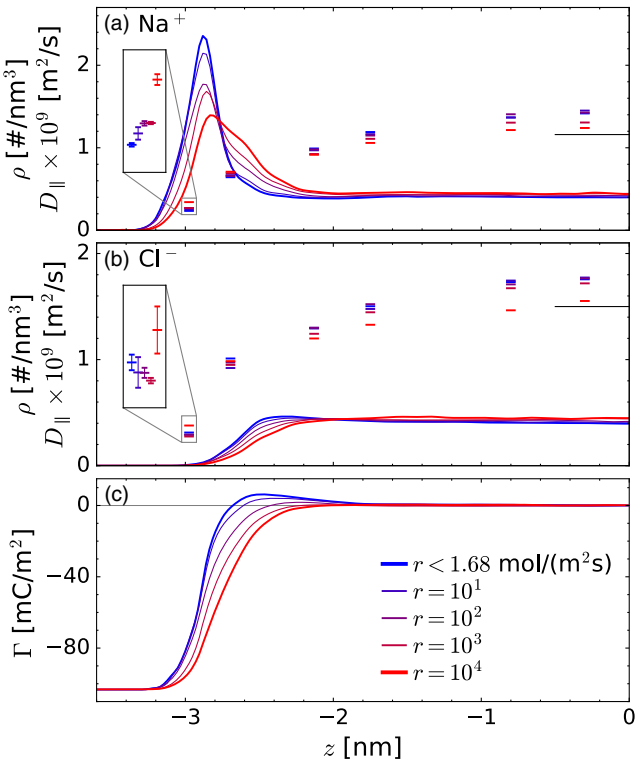

FIG. 2. (a) Na^+ and (b) Cl^- density profiles (lines) and parallel diffusion coefficients (symbols). Symbols in the inset are shifted in z for clarity. Black lines display the bulk diffusion coefficients obtained from independent bulk electrolyte simulations (see Fig. S6 in the Supplemental Material [24] and Refs. [43–45]). (c) Screening function Γ. $z = 0$ is the channel center.

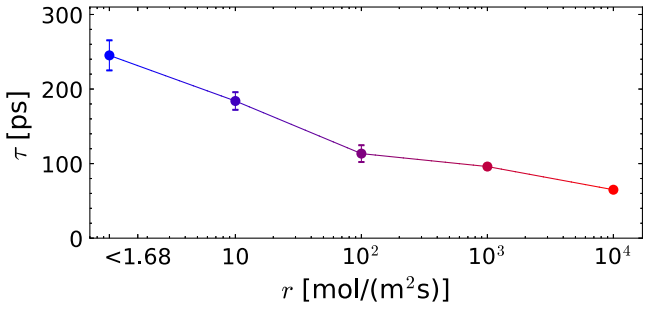

FIG. 3. Mean adsorption, i.e., residence times, $\tau = \int p_\tau dt$ (see Fig. S9 [24]) as a function of r.

Figure 2(a) displays a typical cation density profile obtained in MD simulations of silica-electrolyte interfaces. Upon increasing the protolysis rate r, the cation peak in the density profile decreases, broadens and shifts away from the surface. These changes are consistent with a shift from predominantly specific to predominantly nonspecific cation adsorption as demonstrated in Fig. S10a of Ref. [24]. In other words, for large r, the average time for Na^+ ions to adsorb may exceed the characteristic reprotonation time of a deprotonated site (SiO^- density$/r$, see Table SI [24]). From the cation perspective, the surface charge effectively becomes more uniformly distributed as r increases. This results in the reduction of specifically adsorbed cations. As expected with less specific cation adsorption, anion adsorption is less pronounced [Fig. 2(b)] while water molecules are found to orient more strongly towards the surface (Fig. S5b [24]). Apart from this increased hydrophilicity, r is not found to impact the first solvation layer structure and water dynamics (Fig. S5 [24]). Figure 2(a) also shows the parallel diffusion coefficients for cations (perpendicular diffusion coefficients are provided in Fig. S4 [24]). The methodology used to calculate such local diffusivities is described in Sec. SII [24]. These data show that faster desorption and adsorption and the reduction of specifically adsorbed cations, as induced by higher reaction rates r, lead to faster ion dynamics in the EDL. On the one hand, nonspecifically adsorbed cations are more mobile, and on the other hand, as some cations quickly desorb from protonating SiO^- sites, other cations are attracted by deprotonating SiOH sites as illustrated in Fig. 1(b). Consequently, upon increasing the protolysis rate r, the cation diffusion coefficients near the surface increase [inset in Figs. 2(a) and S4b [24]], while the average Na^+ residence time decreases (Fig. 3). Since barely any anions specifically adsorb, their diffusion coefficients do not show any dependence on r [Figs. 2(b) and S4c [24]]. Similarly, water diffusion coefficients and fluid viscosity are found to be nearly rate independent [Figs. S4a and S5(a),(c) [24]].

Using the Boltzmann equation, the ion density profile can be written as $\rho(\mathbf{x}) = \rho(\infty)\exp[-\beta\mathcal{F}_r(\mathbf{x})]$, where $\beta = 1/k_BT$, $\rho(\infty)$ is the bulk density and $\mathcal{F}_r(\mathbf{x})$ is the free energy landscape at a given rate r. Considering an energy landscape possessing different adsorption sites, the density profile in z follows $\rho(z) = (L_xL_y)^{-1}\int\int\rho(\infty)\times\exp[-\beta\mathcal{F}_r(x,y,z)]dxdy$, where the integrals run over the surface area. This expression can be considered in asymptotic limits depending on the reaction rate r and characteristic time τ_e over which cations relax towards local equilibrium. For $r\tau_e \ll 1$, the surface can be considered "quenched" (nonreactive). In this case, the surface contains a fraction $\alpha_\bullet$ of protonated sites MOH and a fraction $\alpha_\circ = 1 - \alpha_\bullet$ of deprotonated sites MO^- such that the density follows $\rho(z) = \rho(\infty)\langle\exp[-\beta\mathcal{F}_r(z)]\rangle$, where $\exp[-\beta\mathcal{F}_r(z)] = \alpha_\bullet\exp[-\beta\mathcal{F}_\bullet(z)] + \alpha_\circ\exp[-\beta\mathcal{F}_\circ(z)]$. For $r\tau_e \gg 1$, the surface can be considered "annealed" (reactive). In this case, all surface adsorption sites are equivalent since they frequently switch between protonated and deprotonated. The free energy of these equivalent sites is given by a time average $\beta\mathcal{F}_r(z) = \alpha_\bullet\beta\mathcal{F}_\bullet(z) + \alpha_\circ\beta\mathcal{F}_\circ(z)$ (we use ergodicity to replace the fraction of time spent in one site by its occurrence α). Assuming cations redistribute very fast according to the local free energy landscape, we can write the ion density as $\rho(z) = \rho(\infty)\exp[-\beta\mathcal{F}_r(z)] = \rho(\infty)\exp[-\alpha_\bullet\beta\mathcal{F}_\bullet(z) - \alpha_\circ\beta\mathcal{F}_\circ(z)]$. Provided proper boundary conditions are applied (surface charge and overall charge neutrality), these two limiting cases provide a

framework to rationalize the simulated data. However, beyond such asymptotic cases, obtaining an expression for intermediate reactive rates r is not straightforward as in most situations the corresponding density profile cannot be written as a single contribution (annealed surface) nor as a weighted sum of two independent contributions (quenched surface). Indeed, in these situations, the observed density profile still derives from an underlying energy profile but proper averaging that leads to $\rho(z)$ is ill defined. In particular, in such intermediate situations, there is no clear timescale separation between the relaxation time towards local equilibrium and the typical time between two protonation or deprotonation events so that one obtains density profiles that are rate dependent (in agreement with our simulation data). In the same spirit, one can see the observed density profile broadening as the result of an increased surface self-diffusivity $D_s(z)$. By writing that $D_s(z)$ corresponds to the bulk diffusivity modulated by the surface-ion interaction, one predicts that the impact of reduced surface interactions due to protolysis reactions leads to a larger surface diffusivity [46]. In turn, such enhanced diffusivity leads to surface exploration corresponding to larger mean square displacements through the bulk phase between two relocations (re-adsorption), and hence, broader density profiles near the solid surface.

Upon increasing the reaction rate r, both ion densities increase in the channel center while the ion and water diffusion coefficients decrease [Figs. 2(a), 2(b), and S5a [24]]. Although the EDL net charge is independent of r, the number of ions involved in the EDL decreases upon increasing r. In other words, cations and anions relocate in equal amounts from the EDL to the channel center as r increases. Such relocation would not notably affect bulk ion concentrations in a macroscopic channel. However, as shown in Fig. S1 [24], due to the small pore height $H \approx 6$ nm (approximately 20 times the Debye length, $\lambda_D \sim 0.35$ nm), a concentration increase from 0.66 to 0.74 mol/L can be detected when increasing r to 10^4 mol/m^2/s. As a direct consequence of this concentration increase, the cation, anion, and water diffusion coefficients in the channel center decrease. This is in agreement with data for bulk electrolyte simulations in Fig. S6 of the Supplemental Material [24]. This finite channel size impact on ion concentration and diffusion is expected to become less pronounced as λ_D/H and/or r decrease.

The ion adsorption weakening observed upon increasing r also impacts the screening of the bare surface charge density σ_0. This can best be quantified by assessing the screening function $\Gamma(z) = \sigma_0 + \int_{-\infty}^{z} e[\rho_{Na^+}(z') - \rho_{Cl^-}(z')]dz$. As expected from the change from specific to nonspecific adsorption upon increasing r, the screening peak in Fig. 2(b) shifts away from the surface and decreases in magnitude (the peak even disappears for the fastest rates). Surface reaction kinetics can, thus, directly impact the occurrence of charge inversion ($\Gamma > 0$). This result can explain why many MD studies—carried out with a static surface charge distribution—report charge inversion under conditions for which no experimental charge inversion is found [47–49]. Another reason for such disagreement between MD and experiments may be force field shortcomings as investigated in our recent work [50].

We have thus far shown that reaction kinetics impacts ion adsorption, diffusion and screening of the bare surface charge. Based on these results, a strong impact of protolysis reactions on electrokinetic properties is expected. For example, the ζ potential in Fig. 4(a) is found to decrease with increasing reaction rate r. This result can be explained from changes in the ion density distributions $\rho_{Na^+}(z)$ and $\rho_{Cl^-}(z)$ within the EDL [Figs. 2(a) and 2(b)]. These distributions directly impact the streaming current $I_{str} \sim \int e[\rho_{Na^+}(z') - \rho_{Cl^-}(z')]u_x dz$ and electro-osmotic flow $\eta\nabla^2 u_{\parallel}(z) = e[\rho_{Na^+}(z) - \rho_{Cl^-}(z)]E_x$, which, in turn, fully determine the ζ potential through $\zeta \sim I_{str}/\Delta p_x$ and $\zeta \sim u_{\parallel,bulk}/E_x$ (following Helmholtz-Smoluchowski theory [50,51]). Although the dependence of the ζ potential on the reaction kinetics in Fig. 4(a) appears to be stronger for electro-osmosis than for streaming currents, the ion distributions corresponding to both methods are identical to those shown in Figs. 2(a) and 2(b). Hence, the differences in ζ potential between electro-osmosis and streaming currents must originate from within the Helmholtz-Smoluchowski theory. In fact, in agreement with previous studies [50,52,53], these differences vanish when $\zeta \to 0$,

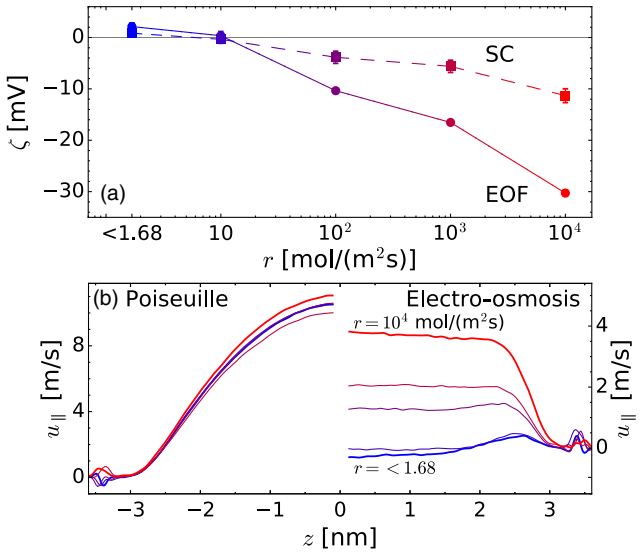

FIG. 4. (a) ζ potential as a function of reaction rate r from streaming current (SC) and electro-osmosis (EOF) simulations. (b) Poiseuille (left) and electro-osmosis (right) flow profiles resulting from a pressure drop of 75 atm and an electric field of 0.2 V/nm. These external forces have been shown to be within the linear response regime [49,50].

which occurs at $r = 10$ mol/m^2/s. It is noteworthy that, since Poiseuille flow depends solely on fluid properties at the center of the channel, velocity profiles corresponding to the streaming currents are independent of r as shown in the left of Fig. 4(b). Conversely, electro-osmotic flow profiles, which are fully determined by the ion distribution within the EDL (following Navier-Stokes equation), change even qualitatively with r as shown in the right of Fig. 4(b).

In summary, we developed a novel framework to account for surface reactions in classical MD simulations at no additional cost compared to nonreactive MD simulations. We then used this method to demonstrate that EDL properties and electrokinetic transport in a silica channel do not just depend on the static surface properties but also on proton exchange reaction kinetics. While such kinetic chemical events are not taken into consideration in available formalisms, we provide strong evidence that such processes affect static and dynamic properties of ions and solvent (water) within porous materials. Specifically, upon increasing the surface reaction kinetics (from no reactivity to rates encountered in experiments), cation adsorption at the negatively charged surface becomes less pronounced with decreased retention times. In turn, such decreased adsorption leads to increased local diffusion coefficients near the solid surface. These changes in ion distribution and dynamics within the EDL also directly impact electrokinetic phenomena with, for instance, the ζ potential reducing upon increasing the protolysis reaction rate. The quantitative and qualitative differences observed between non-reactive and reactive surface charge distributions suggest that such equilibrium surface reactions play an even more important role for the EDL structure and dynamics than has thus far been assumed. In fact, the impact of surface reactivity may even be more pronounced for surface groups with weaker covalent bonds, at higher temperature, lower pH, or for ions with longer residence times, questioning the near-universal neglect of protolysis reactions in simulation and modeling endeavors. Finally, our novel framework provides a stepping stone for more realistic interface modeling within a MD environment, potentially benefiting applications ranging from the design of anticorrosion paints to electrochemical cells. Additional work should also include establishing a bridge between our method and fundamental approaches in which proton creation and diffusion at surfaces is probed [54]. In this context, mesoscopic strategies such as those based on the formalism of intermittent Brownian motion applied to surface adsorption and relocation in pores could prove useful in linking molecular aspects and macroscopic observations [46]. Moreover, to bridge the gap between the microscopic and mesoscopic scales, the inclusion of water ionization reactions from reactive simulations could provide a means to account for chemical events occurring at the fs time scale.

The scripts necessary to reproduce this work can be found on GitLab [55]. B. C. is grateful to Vivien Lecomte for the stimulating discussion. This work was carried out on the Dutch national e-infrastructure with the support of SURF Cooperative.

*r.m.hartkamp@tudelft.nl

[1] J. Lyklema, *Fundamentals of Interface and Colloid Science: Soft Colloids* (Elsevier, New York, 2005), Vol. 5.
[2] M. Nogami, R. Nagao, and C. Wong, J. Phys. Chem. B **102**, 5772 (1998).
[3] N. Amdursky, Y. Lin, N. Aho, and G. Groenhof, Proc. Natl. Acad. Sci. U.S.A. **116**, 2443 (2019).
[4] M. Ashida, M. Sasaki, H. Kan, T. Yasunaga, K. Hachiya, and T. Inoue, J. Colloid Interface Sci. **67**, 219 (1978).
[5] L. R. J. Scarratt, K. Kubiak, P. Maroni, G. Trefalt, and M. Borkovec, Langmuir **36**, 14443 (2020).
[6] D. Lis, E. H. G. Backus, J. Hunger, S. H. Parekh, and M. Bonn, Science **344**, 1138 (2014).
[7] B. L. Werkhoven, J. C. Everts, S. Samin, and R. van Roij, Phys. Rev. Lett. **120**, 264502 (2018).
[8] P. Ober, W. Q. Boon, M. Dijkstra, E. H. Backus, R. van Roij, and M. Bonn, Nat. Commun. **12**, 4102 (2021).
[9] M. Kagan, G. K. Lockwood, and S. H. Garofalini, Phys. Chem. Chem. Phys. **16**, 9294 (2014).
[10] B. M. Lowe, C.-K. Skylaris, and N. G. Green, J. Colloid Interface Sci. **451**, 231 (2015).
[11] P. M. Dove and C. J. Nix, Geochim. Cosmochim. Acta **61**, 3329 (1997).
[12] S. A. Carroll, R. S. Maxwell, W. Bourcier, S. Martin, and S. Hulsey, Geochim. Cosmochim. Acta **66**, 913 (2002).
[13] M. Wilson and T. R. Walsh, J. Chem. Phys. **113**, 9180 (2000).
[14] T. R. Walsh, M. Wilson, and A. P. Sutton, J. Chem. Phys. **113**, 9191 (2000).
[15] H.-P. Cheng, R. N. Barnett, and U. Landman, J. Chem. Phys. **116**, 9300 (2002).
[16] C. Mischler, J. Horbach, W. Kob, and K. Binder, J. Phys. Condens. Matter **17**, 4005 (2005).
[17] Y.-W. Chen and H.-P. Cheng, J. Chem. Phys. **134**, 114703 (2011).
[18] A. C. T. van Duin, S. Dasgupta, F. Lorant, and W. A. Goddard, J. Phys. Chem. A **105**, 9396 (2001).
[19] T. S. Mahadevan and S. H. Garofalini, J. Phys. Chem. B **111**, 8919 (2007).
[20] T. S. Mahadevan and S. H. Garofalini, J. Phys. Chem. C **112**, 1507 (2008).
[21] G. K. Lockwood and S. H. Garofalini, J. Phys. Chem. C **118**, 29750 (2014).
[22] T. S. Mahadevan and J. Du, J. Am. Ceram. Soc. **103**, 3676 (2020).
[23] S. Plimpton, J. Comput. Phys. **117**, 1 (1995).
[24] See Supplemental Material at http://link.aps.org/supplemental/10.1103/PhysRevLett.128.056001 for details on the molecular dynamics simulations, theoretical framework to calculate the local diffusion coefficients, details on the electrokinetic theory and additional results.

[25] B. W. H. van Beest, G. J. Kramer, and R. A. van Santen, Phys. Rev. Lett. **64**, 1955 (1990).
[26] K. Vollmayr, W. Kob, and K. Binder, Phys. Rev. B **54**, 15808 (1996).
[27] J. Geske, B. Drossel, and M. Vogel, AIP Adv. **6**, 035131 (2016).
[28] R. L. Mozzi and B. E. Warren, J. Appl. Crystallogr. **2**, 164 (1969).
[29] J. H. Konnert and J. Karle, Acta Crystallogr. Sect. A **29**, 702 (1973).
[30] D. I. Grimley, A. C. Wright, and R. N. Sinclair, J. Non-Cryst. Solids **119**, 49 (1990).
[31] N. R. Haria and C. D. Lorenz, Phys. Chem. Chem. Phys. **14**, 5935 (2012).
[32] F. S. Emami, V. Puddu, R. J. Berry, V. Varshney, S. V. Patwardhan, C. C. Perry, and H. Heinz, Chem. Mater. **26**, 2647 (2014).
[33] S. Halbert, S. Ispas, C. Raynaud, and O. Eisenstein, New J. Chem. **42**, 1356 (2018).
[34] L. T. Zhuravlev, Colloids Surf. A **173**, 1 (2000).
[35] P. Ugliengo, M. Sodupe, F. Musso, I. J. Bush, R. Orlando, and R. Dovesi, Adv. Mater. **20**, 4579 (2008).
[36] S. H. Garofalini, J. Non-Cryst. Solids **120**, 1 (1990).
[37] A. Comas-Vives, Phys. Chem. Chem. Phys. **18**, 7475 (2016).
[38] H. J. C. Berendsen, J. R. Grigera, and T. P. Straatsma, J. Phys. Chem. **91**, 6269 (1987).
[39] I. S. Joung and T. E. Cheatham, J. Phys. Chem. B **112**, 9020 (2008).
[40] J. Lützenkirchen, T. Preočanin, D. Kovačevič, V. Tomišić, L. Lövgren, and N. Kallay, Croat. Chem. Acta **85**, 391 (2012).
[41] M. Rezaei, A. R. Azimian, A. R. Pishevar, and D. J. Bonthuis, Phys. Chem. Chem. Phys. **20**, 22517 (2018).
[42] I. C. Yeh and M. L. Berkowitz, J. Chem. Phys. **111**, 3155 (1999).
[43] M. F. Döpke, O. A. Moultos, and R. Hartkamp, J. Chem. Phys. **152**, 024501 (2020).
[44] G. Guevara-Carrion, J. Vrabec, and H. Hasse, J. Chem. Phys. **134**, 074508 (2011).
[45] J. S. Kim, Z. Wu, A. R. Morrow, A. Yethiraj, and A. Yethiraj, J. Phys. Chem. B **116**, 12007 (2012).
[46] C. Bousige, P. Levitz, and B. Coasne, Nat. Commun. **12**, 1043 (2021).
[47] R. Hartkamp, B. Siboulet, J.-F. Dufrêche, and B. Coasne, Phys. Chem. Chem. Phys. **17**, 24683 (2015).
[48] M. F. Döpke, J. Lützenkirchen, O. A. Moultos, B. Siboulet, J.-F. Dufrêche, J. T. Padding, and R. Hartkamp, J. Phys. Chem. C **123**, 16711 (2019).
[49] N. R. Haria and C. D. Lorenz, J. Phys. Chem. C **119**, 12298 (2015).
[50] M. F. Döpke and R. Hartkamp, J. Chem. Phys. **154**, 094701 (2021).
[51] A. Delgado, F. González-Caballero, R. Hunter, L. Koopal, and J. Lyklema, J. Colloid Interface Sci. **309**, 194 (2007).
[52] A. Szymczyk, P. Fievet, M. Mullet, J. Reggiani, and J. Pagetti, J. Membr. Sci. **143**, 189 (1998).
[53] G. Hurwitz, G. R. Guillen, and E. M. Hoek, J. Membr. Sci. **349**, 349 (2010).
[54] J. Comtet, B. Grosjean, E. Glushkov, A. Avsar, K. Watanabe, T. Taniguchi, R. Vuilleumier, M.-L. Bocquet, and A. Radenovic, Nat. Nanotechnol. **15**, 598 (2020).
[55] See Python and LAMMPS scripts at [https://gitlab.com/mdopke/surfacereactions].